Flexural Failure of Fabric Reinforced Cementitious Mortar (FRCM) Plates under Punctual Loads: experimental test, analytical approach and numerical simulation

Luis Mercedes [(1)], Ernest Bernat-Maso [(1)(3)], Lluis Gil [(1)]

[(1)] Department of Strength of Materials, Polytechnic University of Catalonia, Terrassa, Spain

[(2)] LITEM Laboratory for Technological Innovation of Structures and Materials, Spain

[(3)] Serra Húnter Fellow

Abstract

Fabric-reinforced cementitious matrix (FCRMs) are composites that produce lighter and more durable strengthening solutions. In this study, carbon and basalt fabrics were used to manufactured FRCM plate specimens. These plates were subjected to a centered punctual load with different punch diameters. Flexural failure mode was observed. Experimental tests showed that carbon and basalt fabrics improved notably the load capacity and the stiffness of mortar plates compared to unreinforced ones. Moreover, failure in the reinforced plates was progressive, preventing the sudden brittle failure of the unreinforced ones. Analytical and numerical models were adjusted and validated from experimental results, and both have proved to be effective calculation tools. What is more, numerical model allowed to determine a sliding tensile stress for the carbon fabric used in this study.

Keywords: Plates, FRCM, Cementitious matrix, Carbon fibres, Basalt fibres, Flexural test, Analytical model, Numerical model

1 Introduction

Concrete plates or slabs are one of the most used structural elements in building construction, especially the well-known concrete reinforced flat slabs, that give the advantages of providing more free space [1].

The problem of concrete plates subjected to punctual loads has been studied from the very beginning. Punctual loads may produce flexural failures but also punching failures, which are sudden and extremely dangerous. The transition way one to other is not clear and there are still a lot of research about this issues.

Currently, there are some articles aimed at studying the behavior of reinforced cementitious matrix plates, see [2][3]. Of particular interest is the work of [4], this paper presented experimental tests conducted on square cementitious slabs simply supported on four edges and subjected to patch load. The test results showed that adding a wire mesh to ordinary reinforcement increases significantly the punching resistance. Moreover, as the loaded area size increases both ductility and stiffness increase and the bridging effect due to the difference in the reinforcement ratio in orthogonal directions was clearly noticed.

In order to know the difference between flexural and punching failure, the research presented by [5] carry out an experimental campaign. In this was observed that the failure load is raised with increasing cross-section of the reinforcement. The load–displacement curves illustrated that after the maximum load was reached, a flexural failure is characterized by a smooth decrease of the carrying load with increasing displacement. In the opposite case, a punching failure results in a sudden decrease of the carrying load after the maximum load. These results clearly illustrate the difference between both failure mechanisms for traditional steel reinforcement.

The fabric cementitious matrix (FRCM) is well known as a strengthening system used to improve the mechanical behavior from structural elements [6][7][8][9][10][11][12]. This emerged as a promising alternative to organic matrix based fibre reinforced polymers (FRPs), and also this is an evolution of ferrocement used for manufacturing plate or flat slab.

FRCM consists of a fabric embedded in an inorganic mortar matrix. This fabric can be made of diverse materials such as glass, carbon, basalt [13,14], PBO (Polyparaphenylene benzobisoxazole), and vegetal fibre [15].
It is essential to understand that FRCM provides tensile strength thanks to the fabrics, and that these fibres only bear the loads that the mortar is capable of transmitting [16]. Therefore, the transmission of matrix-mesh stresses is one of the main requirements to be considered, as well as the geometric adaptability of the fabric and its chemical stability (durability) within the matrix.
In the case of cementitious plates with fabrics of synthetic fibres, in the research presented by [17], specimens of carbon fabric reinforced cementitious matrix (FRCM) with chopped carbon fibre were developed. A series of three-point bending tests were conducted to investigate the effects of chopped carbon fibre content and the carbon mesh. The results show that the carbon mesh is effective as reinforcement of cementitious matrix, where during in the bending test the loads of the specimens continued to increase after the occurrence of visible cracks, which indicated that the carbon mesh in the center of FRCM plates enhances the plasticity of cementitious matrix.
From the studies presented above, it can be seen that most of these investigations are aimed at the study of steel reinforced concrete plates whereas it seems there are no records of experimental campaigns aimed to demonstrate the flexural behavior of FRCM plates. The present work is an experimental campaign aimed to analyze the behavior of different FRCM materials (carbon and basalt fibres) in the shape of small plates. From the test results it is aimed to develop analytical and numerical models capable of reproducing the flexural failure of FRCM plates under simple supported boundary conditions. It is expected that this study will raise the possibility of replacing steel with synthetic fiber fabrics, which would reduce the thickness of the plates, making them lighter and avoiding the durability drawbacks caused by the steel corrosion. Nevertheless, the investigation is mainly oriented to the material performance and results are prevented to be directly extended to real size slabs.

2 Materials and specimens

In order to face the experimental campaign some samples of small FRCM plates were produced according next conditions.

2.1 Mortar

A single type of commercial mortar was used in this study. It was an auto-levelling mortar which includes organic additives (plasticiser polymer). The manufacturing of samples was performed with a single batch and some test on compression and flexural. The control mortar specimens were tested to flexion in an electromechanical press of 50 kN, and then the resulting halves were tested under compression with a hydraulic actuator of 100 kN capacity. These tests were performed according to EN 1015-11: 2000 [18].

Table 1. Mortar properties

Mortar	***Flexural strength (MPa)***		***Compressive strength (MPa)***	
	Average	*C.V.*	*Average*	*C.V.*
A	8.84	(11%)	36.60	(7%)

2.2 Fabrics

Two type of fabrics were used to manufacture the FRCM plates: carbon and basalt fibres. The averaged results of a tensile tests and other mechanical properties (supplied by the manufacturer) are summarized in Table 2. These experimental data were previously determined in [19] and they were obtained from tests of 5 tows of the each fabric (carbon and basalt) using the same procedure presented in [20].

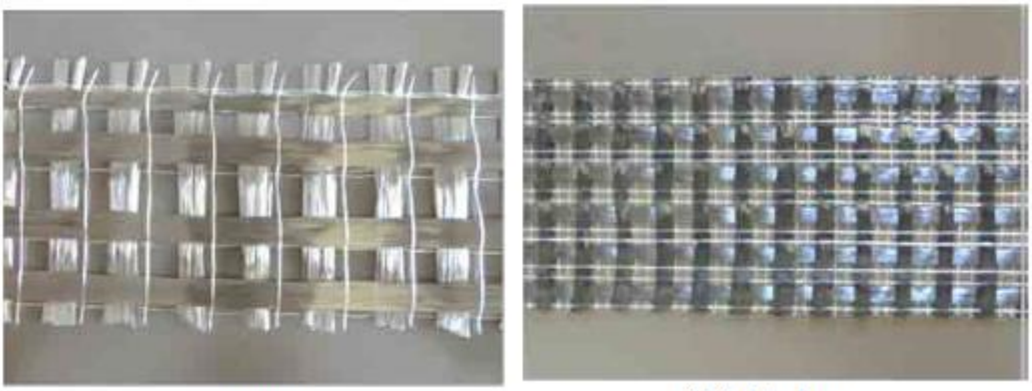

Figure 1. Fabrics

Table 2. Fibres and fabric properties

	Property	Units	Basalt (B)	Carbon (C)
Fibres	Ultimate tensile strength(1)	$f_{fib,u}$ [MPa]	3080	4320
	Elastic modulus(1)	E_{fib} [GPa]	95	240
	Ultimate strain(1)	$\varepsilon_{fib,u}$ [%]	3.15	1.80
Fabric	Fibre orientation(1)		Bidirectional	Bidirectional
	Equivalent thickness(1)	t_{tex} [mm]	0.053	0.047
	Distance between tows(1)	d_{tows} [mm x mm]	15x15	10x10
	Elastic modulus(2)	E_{tex} [GPa]	87.81	235.69
	Ultimate tensile strength(2)	$f_{fab,u}$ [MPa]	763.7	1915.74

(1) Supplied by manufacturer; (2) results of tensile test [19].

2.3 Specimens

The experimental program included 27 samples of FRCM plates. There is no specific norm about specimen dimensions for assessing the response to a punctual centered load. The closer to this research might be a reference related to punching shear on ferrocement by [4]. This author used plates of effective dimensions 400 mm x 400 mm with thickness from 40 to 60 mm. He reinforced slabs with a wire mesh and some steel rods. In the present research the reinforcement is by fabric, with less strength than steel reinforcement. Therefore the dimensions of the specimens can be taken half of 400 mm that is enough to create a relevant flexural deformation. Hence, every plate had dimensions of 200 mm x 200 mm and a thickness of 20 mm.

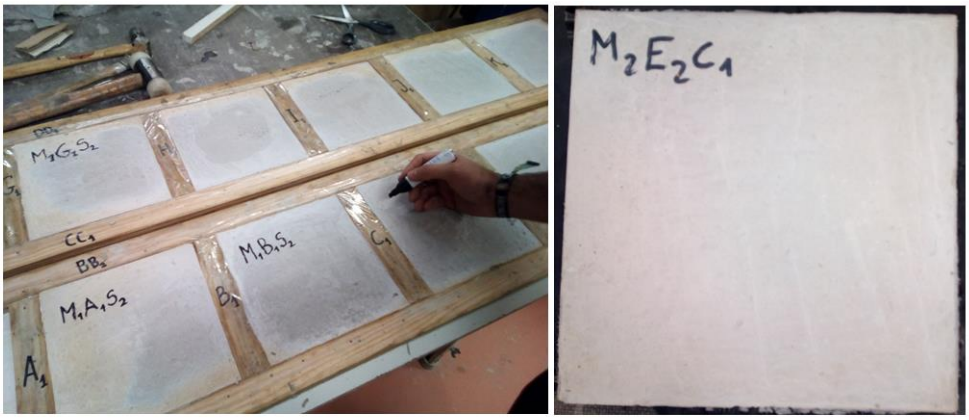

Figure 2. Manufacturing of specimens and traceability labels

There were three types of plates, the ones without any reinforcement, the ones with carbon fabric and finally, the ones with basalt fabric. One of the objectives was to compare the different performance according the nature of fabric.

All plates were manufactured at the same time in a single batch in three molds. Every mold produced all plates of the same type. Each specimen is labeled with the reinforcement material: None, Carbon or Basalt and the punching diameter: D16, D30, D63 in this manuscript.

Every mold was prepared with a grid of wooden strips defining 200 mm x 200 mm gaps. These strips had only a height of 10 mm, just the half of the total plate thickness, so to place one continuous reinforcement fabric for all the plates in a mold. Fabric was placed "as-it-is". Therefore, bonding was only achieved by chemical and friction with no special treatment or mechanical device placed at the edge of the samples. A second layer of wooden strips was placed on the first one to reach the 20mm plate thickness. The manufacturing procedure was as follows:

- ✓ Preparing the mold basis with demolding agent.
- ✓ Mixing the mortar and pouring it up to fill the mold and level it. For unreinforced plates the procedure was over.
- ✓ Cover the whole mold with the reinforcement grid and bond it lightly to the wooden strips using stitches and adhesive tape.
- ✓ Place a second layer of wooden strips and nail them lightly to the mold.
- ✓ Pour mortar up to fill the mold and level it.
- ✓ Manually shake the mold to vibrate mortar.
- ✓ Cover the mold with a plastic cover to maintain moisture. And keep it in laboratory conditions for 10 days.
- ✓ Demold and leave samples to cure in laboratory conditions for other 18 days. After that the plates were ready to be tested

All samples were measured to ensure the proper dimensions. It was found that square size was perfect but thickness had some small deviations at a certain point, less than 1 mm, and it was considered acceptable (less than 5%).

3 Experimental campaign

3.1 Test setup and instrumentation

The test is based on placing the plate over a rigid boundary frame and press the top surface with a concentrate load. Load is applied with a cylindrical tool in the middle of the sample. For each type of plate three different punching tools were used. One with diameter 15.9 mm (named D16), other 30 mm (named D30) and finally, 63.5 mm (named D63).

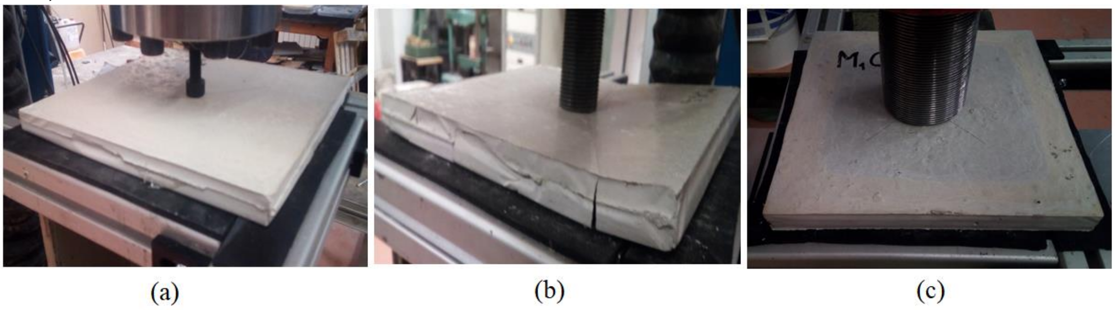

Figure 3. Test setup: (a) D16, (b) D30, (C) D63

Rigid frame was made of connected aluminium profiles. In the contact between the plate and the frame a very thin rubber strip was placed to avoid stress concentrators that may modify the crack pattern. Plate was simply supported at every edge (see Figure 3).
A universal electromechanical machine applied the load with displacement control at a speed 1mm/s. Continuous measurement included displacement and load from the machine sensors. The test ended when the load decreases 10% of the peak load.

3.2 Experimental results

3.2.1 Crack patterns

The results of the different tests are shown in Figure 4. In all tests first cracks started at the bottom side of the specimen under the loading area. Later cracks propagated diagonally to the boundary condition. The crack pattern followed the classical distribution of a yield line flexural failure.
The FRCM-plates presented two type of failures:

- ✓ Fabric sliding failures [21,22]: this occurred in carbon-FRCM, where the fabric starts to slide when the maximum load was reached. This showed that the bonding interaction between fabric-mortar was not perfect (mortar debonding, see Figure 4. Carbon D16, D30, D63) after the fabric reached some sliding tensile stress.
- ✓ Fabric rupture failures: this occurred in the basalt-FRCM, where the fabric reach its tensile strength. Final crack thickness is wider than for carbon-FRCM specimens (see Figure 4. Basalt D16, D30, D63). This means perfect interaction between the fabric and the mortar.

The unreinforced specimens break with a sudden mechanism. As soon as the yield lines appeared, the sample broke down. Little number of wide cracks were developed (see Figure 4. None D16, D30, D63). On the contrary, all reinforced specimens showed a smooth decrease in the applied load while the cracks grew and developed.

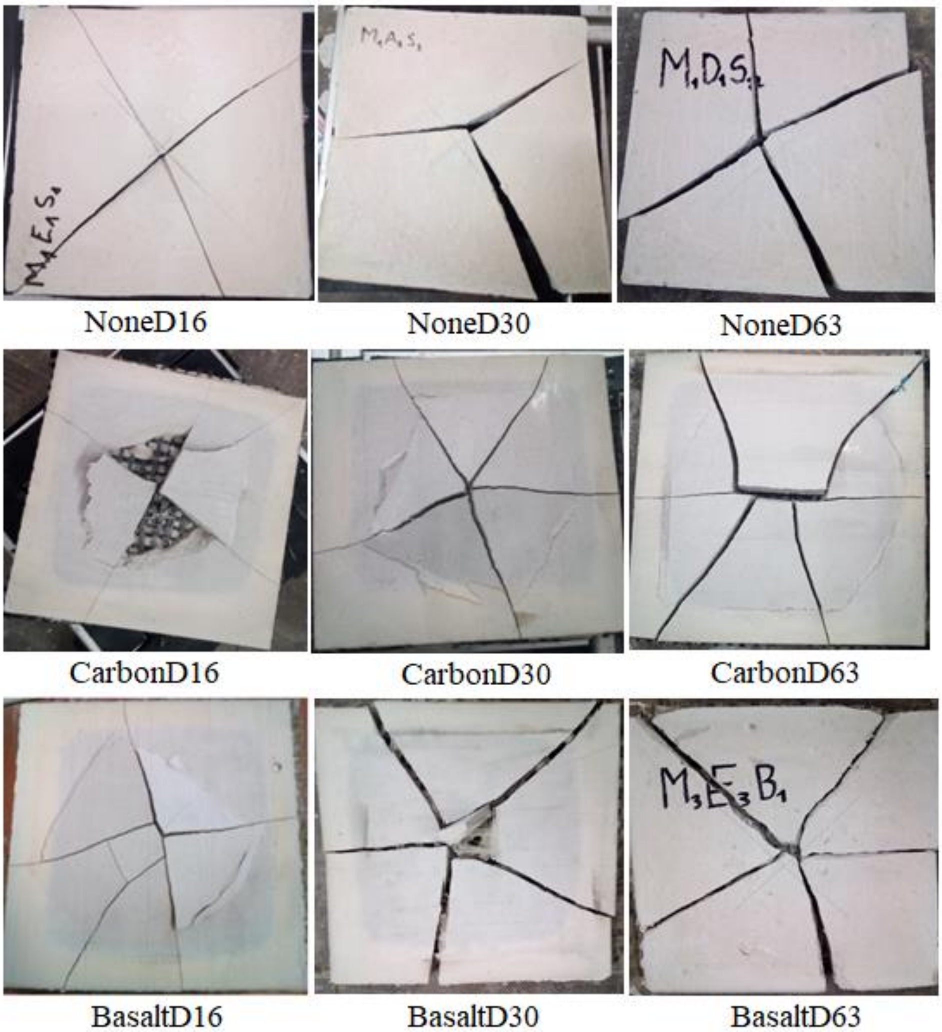

Figure 4. Crack pattern

3.2.2 Maximum load and stiffness coefficient

Table 3 shows the experimental results of maximum load (P_{max}) and the initial stiffness coefficient (K_i) for all the specimens. The initial stiffness was calculated from the first slope in the load-displacement curve presented in Figure 6.

Table 3.Experimental results

Punch diameter		None		Basalt		Carbon	
		P_{max} (kN)	K_i (kN/mm)	P_{max} (kN)	K_i (kN/mm)	P_{max} (kN)	K_i (kN/mm)
D16	M1	1.71	4.06	2.15	4.06	2.49	3.65
	M2	1.00	2.90	2.17	3.24	2.22	3.84
	M3	1.16	2.95	2.43	4.16	2.61	4.15
	Average	1.29	3.30	2.25	3.82	2.44	3.88
	C.V.	24%	16%	6%	11%	7%	5%
D30	M1	1.05	2.84	2.39	3.39	2.68	3.29
	M2	1.89	3.80	2.22	4.09	2.55	3.24
	M3	1.92	3.04	2.49	3.57	3.05	4.13
	Average	1.62	3.23	2.37	3.68	2.76	3.56
	C.V.	25%	13%	5%	8%	8%	12%

D63	M1	1.42	2.75	2.84	4.27	3.97	2.64
	M2	2.44	3.30	3.19	3.37	3.73	4.54
	M3	1.82	3.76	3.14	3.87	3.82	3.54
	Average	1.89	3.27	3.06	3.84	3.84	3.57
	C.V.	22%	13%	5%	10%	3%	22%

The results presented in Table 3 show coefficients of variation between 3% and 25%. The unreinforced samples showed the greatest scattering of data, as it was expected for a single mortar material. On the contrary, the reinforced ones limited its scattering at 10% which represents good repeatability of the experiments.

Figure 5 shows the variation of the maximum load and initial stiffness for each type of specimen and punch diameter. In Figure 5a, it is appreciated that the maximum load increased with the increase of the punch diameter. The load-bearing capacity was greater for larger punch diameter because the punch area was nearer to the support, so to reach the same flexural moment it was necessary to apply a greater load. Also Figure 5a shows that the basalt and carbon fabrics increased the maximum load in all the specimens, especially in the case of carbon-FRCM (D63) where this improved 103%.

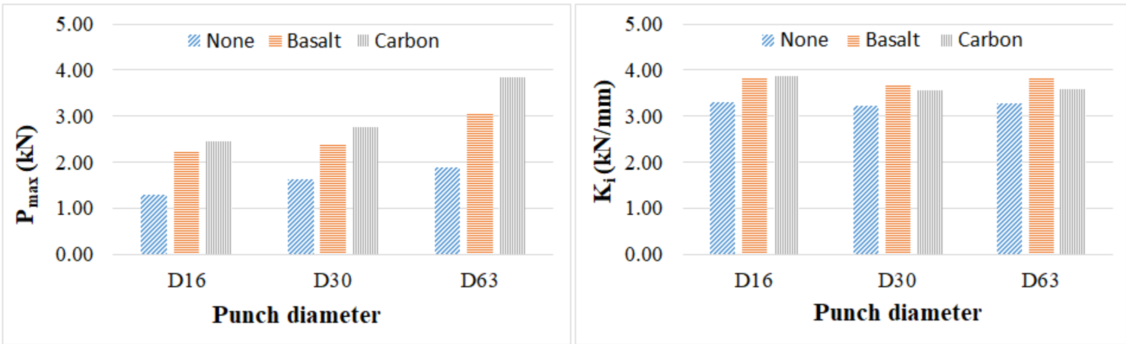

(a) (b)

Figure 5. Experimental results

Figure 5b shows a negligible change (slightly larger) of the initial stiffness in the FRCM plates compared to the plates without fabric. Basalt and carbon FRCM did not contribute with significant stiffness. This is an expected result because the reinforcement modifies the strength of the specimen but its deformation depends mostly on the mortar stiffness and the specimen geometric inertia, two parameters that the fabric did not modify.

Figure 6 show the average of the load-displacement curves of the experimental results. In the case of unreinforced plates (“none” in Figure 6) it is shows a sudden decrease of the carrying load after the maximum loads, in change in the case of FRCM specimen it is shows a smooth decrease of the carrying load when the maximum loads is reached [5], this is due to friction between materials that prevents brittle breakage and dissipates more energy. This confirms the flexural failures showed in the specimens (Figure 4).

Also in the case of FRCM specimen Figure 6 shows a first slope where the fabric and the mortar have the same deformation, however when the mortar reach the carking stress, they start a stage of fabric-mortar interaction, and after that there are a stiffness change controlled by the fabric stiffness. This behavior meets the three lineal tensile model presented by [23].

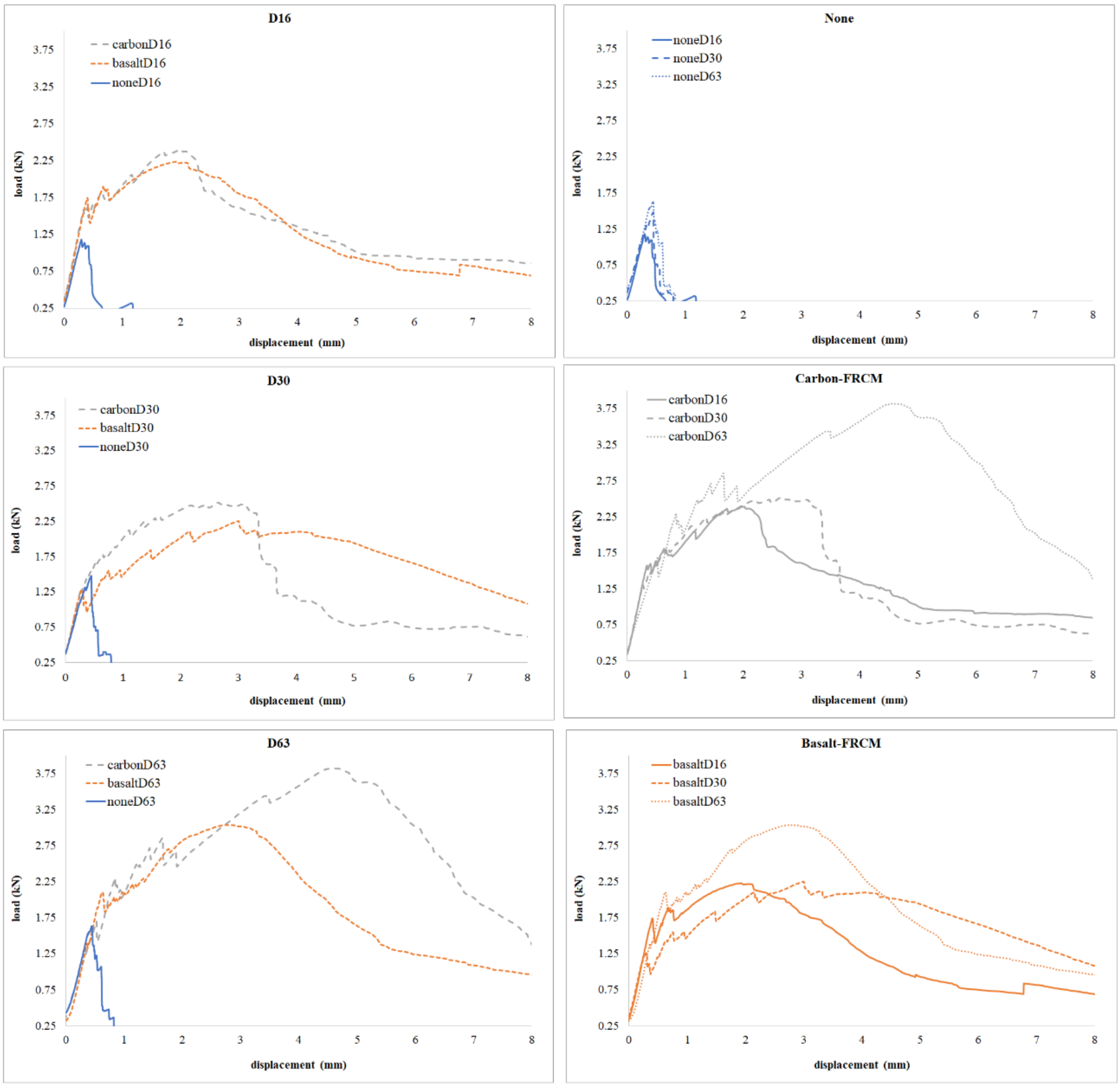

Figure 6. Average of the experimental load-displacement plots

4 Analytical model

4.1. Analytical unreinforced model

In the case of unreinforced plate, the symmetric model presented in Figure 7 was considered, from this model it was possible to obtain the following equations (eq. 1-2).

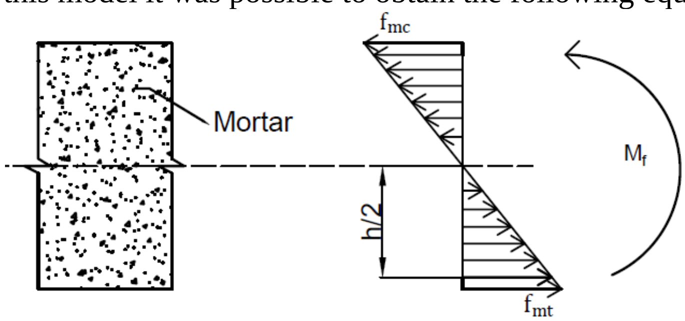

Figure 7. Analysis of cross-section for unreinforced section

Constitutive behaviour of concrete (mortar for this case), is shown in Figure 7 and Figure 8 and according to classical plate theory of yield lines of Johansen.

Where the maximum force (F_{max}) is:

$$F_{max} = \frac{f_{mt,u} h}{4} \qquad \text{Eq. 1}$$

$$M_u = F_{max} \times d \qquad \text{Eq. 2}$$

$$d = \frac{2h}{3} \qquad \text{Eq. 3}$$

$f_{mt,u}$: is the tensile strength
M_u: is the ultimate moment
d: is the distance since the concentrate maximum force until the neutral fiber (lever arm)

The tensile strength was determined from the equation 4 until 7 (which were extracted from the yield lines method presented in Figure 8). This was possible with the maximum load (p) obtained from the experimental test.

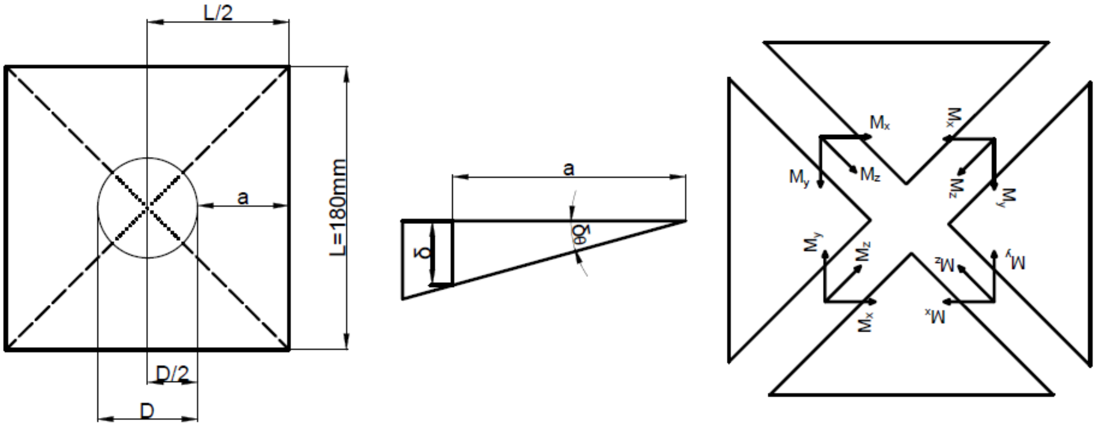

Figure 8. scheme representative based in yield lines plate theory

$$U = 4 \times M_u \times L \times \delta_\theta \qquad \text{Eq. 4}$$

$$\delta_\theta = \frac{\delta}{a} \qquad \text{Eq. 5}$$

$$W = p \times \delta \qquad \text{Eq. 6}$$

$$p = \frac{4 \times M_u \times L}{a} \qquad \text{Eq. 7}$$

Where:
U: is the sectional theory energy
δ_θ: is the angular distortion (Figure 8)
δ: is the vertical displacement (Figure 8)
a: is the horizontal distance from the plate extreme until the punch extreme (Figure 8)
W: is the work of external forces

From the equations 1-7 was obtained the tensile strength, equivalent to 2.31 MPa, that was validated by the 3 maximum load average obtained experimentally by the 3 different punch used in this study (D16, D30, D63), with percentage variation of 4, 9 and 0 % respectively. This tensile strength was used in the analytical model of the FRCM plates, and their numerical simulation.

4.2. Analytical reinforced model

The analytical method to determine the ultimate flexural capacity of the reinforced plate is based on the following assumptions: (1) strain compatibility during the loading process, (2) equilibrium of forces of the load-bearing cross-section. The mortar tensile strength was not considered, because after the cracks formation the fabric is which support the tensile stress.

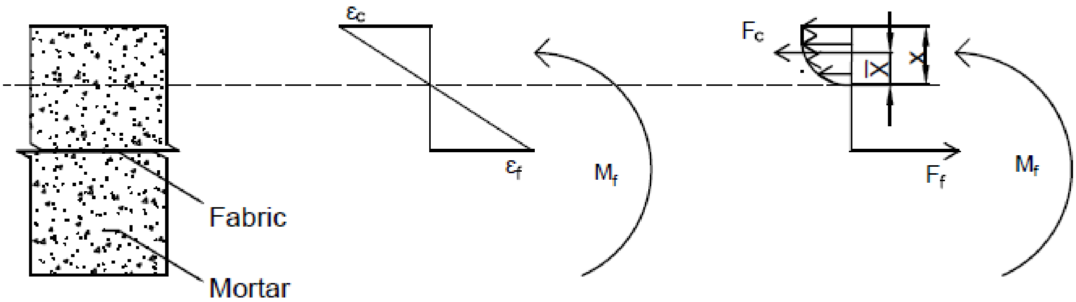

Figure 9.Analysis of cross-section for reinforced section

The proposed analytical approach is based on the assumptions presented in Figure 9. The fabric was assumed to behave linear-elastic until failure, and the stresses in the mortar compression block followed a parabolic-rectangular distribution according to Eurocode [24].

The contribution of the fabric is an effective strength over the total strength of the cross section. Figure 9 shows the internal force equilibrium and the strain distribution of a rectangular FRCM-plate cross-section at maximum bending moment stage. According to Figure 9, the analytical maximum flexural moment ($M_{max,an}$) is calculated as the following (Eq. 1 and 2):

$$M_{max,an} = M_c + M_{fib} \qquad \text{Eq. 8}$$

where M_c and M_{fib} are the ultimate flexural contributions by compression strength of the mortar, and the ultimate flexural contributions of the fibres. The contributions of each withstanding material and neutral axis depth (x) can be determined according to the following equations (Eq. 9 - Eq. 17):

- Ultimate flexural contribution of the compressive stresses on mortar:

$$f_c = f_{cd}\left[1-\left(1-\frac{\varepsilon_c}{\varepsilon_{c0}}\right)^n\right]; if 0 \le \varepsilon_c \le \varepsilon_{c0} \qquad \text{Eq. 9}$$

$$f_c = f_{cd}; if \varepsilon_{c0} \le \varepsilon_c \le \varepsilon_{cu} \qquad \text{Eq. 10}$$

The values of mortar breakage deformation (ε_{c0}) and ultimate deformation (ε_{cu}) in compression are set to 0.002 and 0.0035 respectively, both suggested by Eurocode 2 [24]. These values are valid for concrete with a characteristic compressive strength $f_{ck} \le 50MPa$. Hence the used mortar is assumed to fit into this definition. The compressive strength of the mortar, f_{cd}, as described in section 2.1.

The moment produced by the compression block will be equal:

$$M_c = f_c x \overline{X} \qquad \text{Eq. 11}$$

Where x is the distance from the neutral fiber to most compressed fiber (see Figure 9) and $\underline{x}$ is the distance from center of gravity the compression block to the neutral fiber.

- Ultimate flexural contribution of the fibre fabric:

$$M_{fib} = f_{fib} A_{fib} (h/2 - x) \qquad \text{Eq. 12}$$

It is known that for the tested FRCM-plates the fabrics failure occurred before reaching the maximum compressive mortar deformation. The ultimate fabric deformation ($\varepsilon_{f,u}$, experimental in [19] and Table 2) is taken to calculate the strain in concrete when the maximum load is reached. Strain compatibility is imposed:

$$\varepsilon_c = \frac{\varepsilon_{f,u} . x}{h/2 - x} \qquad \text{Eq. 13}$$

Once the deformations of the materials at the specimens' failure state are known, the following condition must be fulfilled to validate the calculation of the bending capacity of the FRCM-plates:

- ✓ $\varepsilon_c \leq 0.0035$ (Code [24])

4.3. Analytical model results

The results obtained from the analytical model are presented in Table 4. This shows the results of maximum load (P_{max}) and the ultimate flexural moment (M_u) supported by the FRCM-plate. Also, this shows the analytical fabric and mortar ultimate strain when is reached the maximum experimental load of the FRCM-plate.

Table 4. Analytical model results

Punch diameter	**Carbon-FRCM**				**Basalt-FRCM**			
	M_u (MPa)	**P_{max} (KN)**	**ε_f**	**ε_c**	**M_u (MPa)**	**P_{max} (KN)**	**ε_f**	**ε_c**
D16	296.71	2.60	0.0031	0.0008	257.00	2.26	0.0061	0.0011
	-(5%)				(0.4%)			
D30	296.71	2.85			257.00	2.40		
	(3%)				(4%)			
D60	296.71	3.67			257.00	3.09		
	(7%)				(4%)			
(%): variation with the experimental results								

The first data to highlight in Table 4 is that the strain of the carbon fibres are less than the ultimate strain calculated ($\frac{f_{fib}}{E_f} = 0.0031$). This because the fibres sliding before the reach the ultimate strain. The carbon fibres strain presented in table 4 is the 38% of the ultimate carbon strain. In the case of basalt-FRCM the fabric reaches 70% of the ultimate strain, in this case is no reach the ultimate strain, like in the experimental results (fabric rupture).

Also is observed that the mortar ultimate strain (0.0035) is not reached in both cases, whereby, is fulfilled the analytical limit imposed.
The analytical model results were properly approximated to the experimental results, with fitting between 0.4 and 7 % of variation.

5 FRCM numerical simulation

Commercial mechanical simulation software Abaqus® 6.14-4 [26] was used to implement numerical simulations. This choice was based on the aim of using a general purpose-widely available simulation tool that was capable of representing complex material models. In addition, many previous studies for the analysis of FRCM and reinforced concrete successfully used this software (see, for example, [27][28]).

5.1.General material's constitutive formulations

One of the most used approaches for the simulation of FRCM subjected to tensile loads is based on assuming a concrete plastic damage model for cementitious matrix. While fabric is considered an elastic material only dependent from Young's modulus.
Plastic damage model is characterized by the definition of two modulus of elasticity: one corresponding to the elastic zone, and another depending on damage coefficient, which is function of the cracking situation or the plastic degree achieved. In this model, it is assumed that the two main failure mechanisms are tensile cracking and compression crushing of the concrete. The evolution of the yield surface (or failure) is controlled by two plasticity variables ε_t^{pl} y ε_c^{pl}, linked to the failure mechanisms under tension and compression, respectively. These are defined as the plastic deformations equivalent to tension and compression, respectively.
In addition, this model assumes that the strain-stress response for the uniaxial compression of the concrete is characterized by damaged plasticity, as shown in Figure 10. Under uniaxial tension, the stress-strain response follows a linear elastic relationship until the cracking stress value is reached (σ_{t0}). The cracking stress corresponds to the appearance of microcracks in the material. From this point, the tensile tension that transmits the material does not disappear, but it gradually decreases as the deformation increases. Damage variable d_t, whose minimum value is 0 (intact material) and whose maximum value is 1 (totally damaged material), defines the slope of the discharge branch. So, if E_0 is the modulus of elasticity of the elastic material, the module of the discharge branch becomes $(1\text{-}d_t)\ E_0$.
Under uniaxial compression, the response is linear up to the value of initial yield (σ_{c0}). In the plastic zone, the response is typically characterized by stress hardening followed by stress weakening beyond the final stress (σ_u). This representation, although somewhat simplified, captures the main characteristics of the concrete response and it is also valid for mortar. As in the case of tension there is a damage parameter d_t that varies between 0 and 1 which reduces the stiffness of the discharge branch.
This model is useful to simulate the interaction between reinforcement and concrete (fabric and mortar for the case of FRCM), and also provides numerical stability improving convergence.

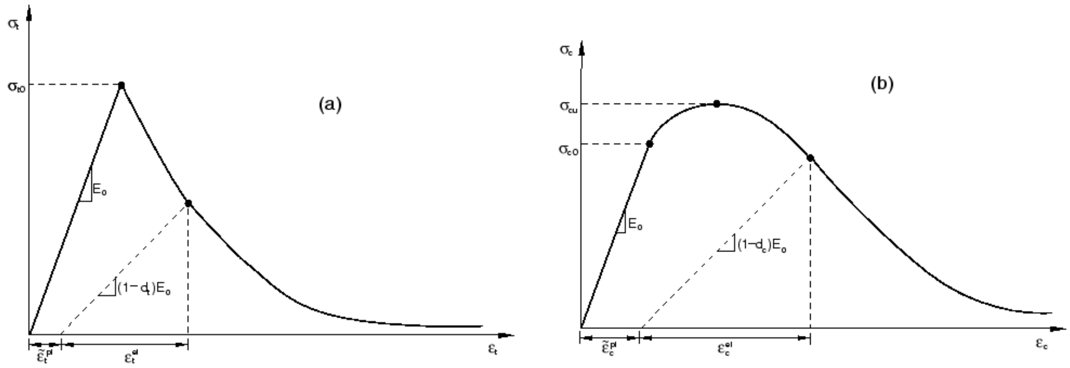

Figure 10. Uniaxial model [26]: (a) tension, (b) compression

5.2. Unreinforced plates modelling

The unreinforced plate specimens were modeled to determine the mortar elasticity modulus and to calibrate the mortar properties for the FRCM-plate simulations. The particularities to model these specimens is described.

First, the geometry of the specimens was defined based on the geometry of the specimens manufactured. These were area of 180×180mm (support positioning) and thickness of 20mm. This geometry was defined as a deformable solid part.

To define the material of the cementitious matrix, the aforementioned plastic damage model was chosen. The elastic behavior of the cementitious matrix was defined by: i) the elasticity model, which was calibrate with the maximum loads and stiffness coefficients obtained experimentally (section) , and ii) the Poisson coefficient, which was set to 0.2 as suggested by EHE [25].

Regarding the plastic zone of the cementitious matrix in tension and compression, it was necessary to define the following parameters:

a) Dilatation angle: This controls the quantity of the plastic volumetric deformation developed during the plastic shear and is assumed constant during the plastic flexibilization. The first value used for this parameter was 13 according [28], but in our simulations we saw that a value of 31 performed better and facilitate the convergence of the computations.
b) Eccentricity: This parameter defines the speed at which the function approaches the maximum stress asymptote. The predetermined eccentricity suggested by Abaqus is 0.1, which implies that the material has almost the same angle of expansion in a significant range of confining pressure values.
c) Form parameter of the plasticizing surface K: This is the ratio of the second invariant tension in the meridian, to that of the compression meridian, in the initial yield for any given value of the invariant pressure. Default value is equal to 2/3.
d) Relationship between the maximum uniaxial and biaxial compression stress at the beginning of the loading process. Default value is equal to 1.16.
e) Viscoplastic regularization: models of materials that exhibit a smoothing behavior and a degradation of rigidity often lead to serious convergence difficulties in implicit analysis programs. A common technique for overcoming some of these convergence difficulties is the use of a viscoplastic regularization of the constitutive equations, which causes the constant tangent stiffness of the softening material to become positive during sufficiently small increments of time. In a range from 0.001 to 0.004, 0.003 proved to be the most stable and provided convergence.

Once these materials properties were defined, the matrix stress-strain curves and the corresponding damage variables were calculated using the procedure from [28].

Next step was defining boundary conditions. The inferior perimeter of the deformable solid was simply supported (restriction of vertical displacements), and the maximum displacement obtained experimentally was imposed on the center of the opposite face, in a superficial circular area, defined by the three different punch diameter used in this study (see Figure 11) .

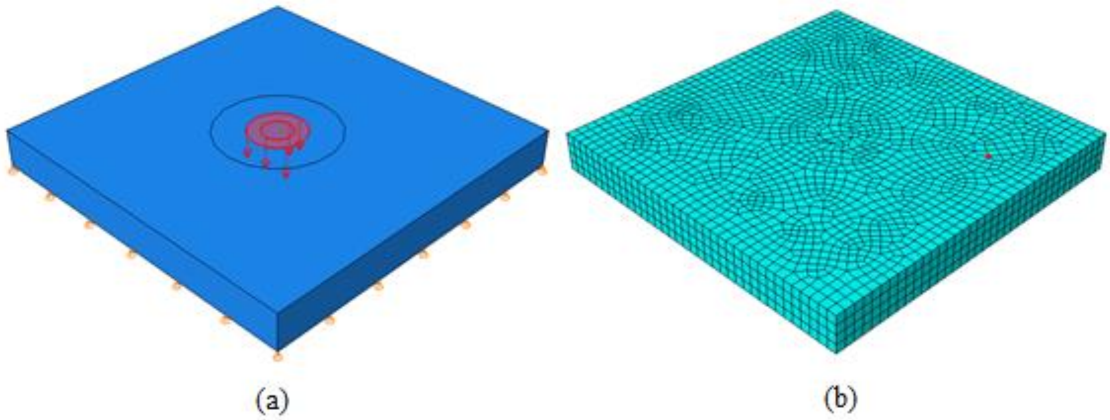

Figure 11. (a) Boundary conditions and (b) Mesh size of deformable solid

Then the mesh was defined. Three meshes of 2.5 mm, 5 mm and 10 mm characteristic size were tested for results convergence analysis, resulting that no significant difference was observed between the results of meshes of 2.5 and 5 mm (2% variation of the maximum load). Hence, the size of elements used was set to 5 mm to reduce calculation cost.

5.2.1. Determining of elasticity modulus of mortar

Mortar’s modulus of elasticity was not known. Hence, it was necessary to calibrate this property with the aim of reproducing the experimental stiffness and maximum load of the unreinforced plates. With this purpose, 4 different moduli for each punch diameter were numerically tested, interpolating or extrapolating the value that best fits experimental results with a parabolic fitting (Figure 12), excepting in the case of the D30 punch, where the results obtained with the modulus of 2388 MPa gave variation with experimental results of 1%. Finally, the three fitted values (one per punch diameter) were averaged. The results are presented in Table 5.

Table 5. Determining of elasticity modulus

	D16		D30		D60	
E (MPa)	**K_i (KN/mm)**	**P_{max} (KN)**	**K_i (KN/mm)**	**P_{max} (KN)**	**K_i (KN/mm)**	**P_{max} (KN)**
2388.00	2.92	1.41	3.19	1.63	4.94	2.21
2089.50	2.69	1.33	-	-	4.41	2.09
1791.00	2.34	1.27	-	-	4.06	1.98
1492.50	2.01	1.19	-	-	3.40	1.85
E_m (MPa)			2098.14			

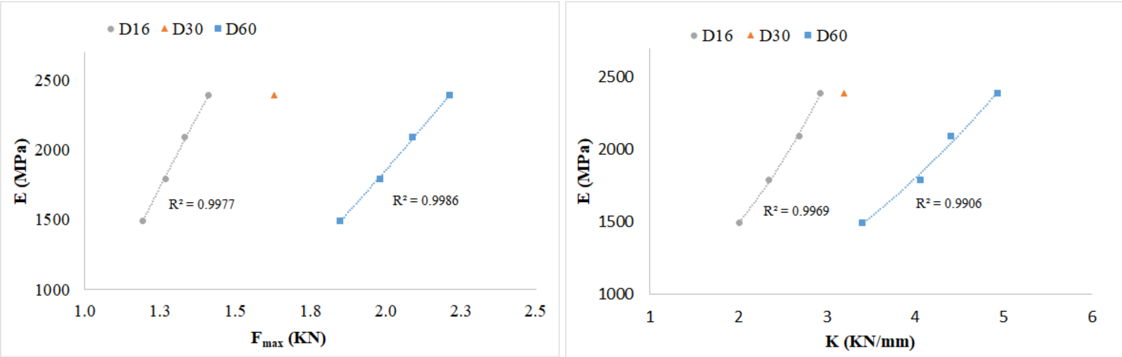

(a) (b)

Figure 12. Tendency of elasticity modulus

5.3.FRCM-plates modelling

Two FRCM-plates were modeled, one for each type of fibres used in the experimental campaign (carbon and basalt). Here, the particularities to model these specimens is described.

The geometry and properties of the deformable solid was the same that the used in the unreinforced plate simulation, with the elasticity modulus previous determined (E_m).

To simulate the fabrics, truss elements were chosen, like in other studies [29]. These are long and thin structural members that can transmit axial force only. These are typically used to model thin, line-like structures that support loading only along the axis or the center line of the element and no moments or forces perpendicular to the center line are considered. Truss elements were used in this case to reduce the high computational costs that the use of three-dimensional elements would cause, as well as to avoid convergence problems.

In carbon-FRCM model, 34 "truss" elements were used (17 in weft direction and 17 in warp direction), and in the basalt-FRCM were used 22 elements (11 in each directions). These simulated tows in the FRCM-plates. These were defined as elastic material, where the Young modulus was the presented in Table 2. Due that the bonding interaction between the mortar and the fabrics was not known, it was considered the fabric totally bonded to the matrix (embedded) without allowing slipping in the fabric-matrix interface. The same boundary condition than for the unreinforced plate were imposed (section 5.2). The mesh size used was set to 5 mm, the same than the deformable solid modelling in section 5.2.

5.4. FRCM-plate results

Figure 13 shows the stress contour plots of the matrix and the reinforcement fabric at the state when the fabric reached the tensile stress taken as failure criterion. The tensile stress taken as failure criteria was determined for each type of fibres by comparing the mean maximum load from the experimental results with the numerical analysis results for each punch size loading. From this initial result it was possible to determine the average tensile stress in the fibres when the numerical analysis reached the experimental maximum load (see Figure 13).

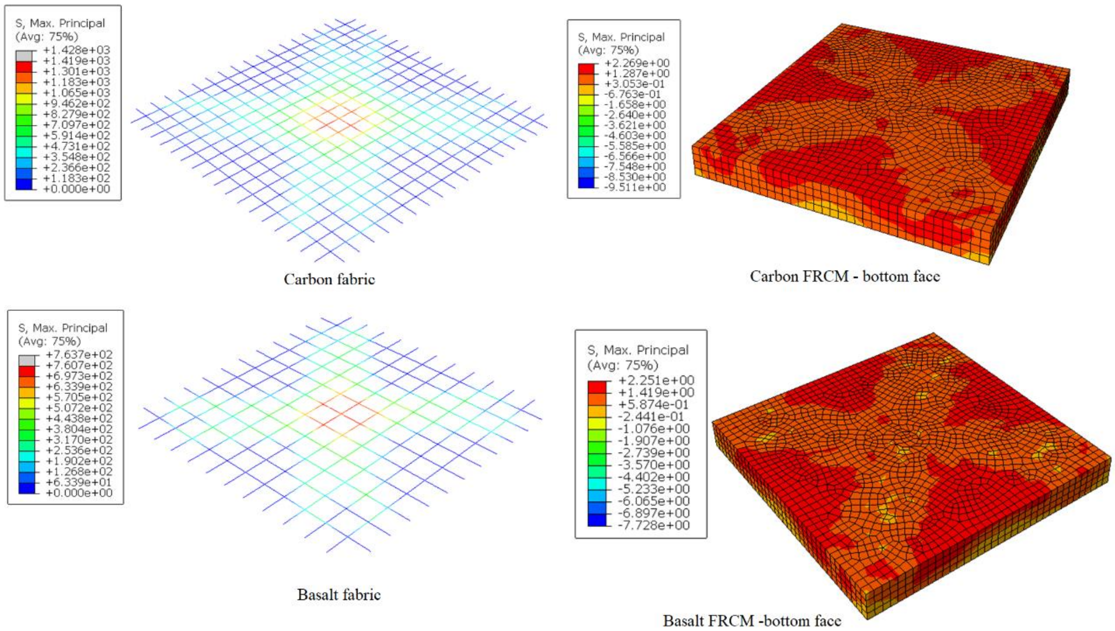

Figure 13. Stress state of the fabric and mortar simulation at the time to reach the failure criteria

The principal stress in the matrix of the FRCM plates shown in Figure 13 describes failures mode similar to the experimental results.

The tensile stress of carbon fabric was 1419.33 MPa (coefficient of variation of 4% for the three punch size used), and 763.7 MPa (0%) for the basalt fabric. These values are 74% of the carbon-fabric tensile strength, and exactly the tensile strength of the basalt-fabric (reaching the tensile rupture). In the case of carbon-FRCM this result can be mean that for this percentage of fabric tension strength, the fabric sliding starts.

The fabric sliding (carbon-FRCM) and the fabric rupture (basalt-FRCM) were the type of failure observed in the experimental campaign (section 3.2.1). Although, in the analytical model (section 4.3) the percentage of carbon tensile strength when the fabric sliding started was 38%. The difference between the numerical and analytical results may be due to the fact that the numerical model considers a full 3D that allows to increase the bidirectional fabric contribution in contrast to the 1D simplification of the analytical model.

Also this sliding failures were presented in a previous experimental tensile study of carbon-FRCM [30], where the sliding tensile stress was 57% of the tensile fabric strength. This mean that the flexural behavior of the FRCM-plate improves 17% the fabric sliding stress, maybe because of the out-of plane normal stress induced friction.

The results obtained from the numerical model are presented in Table 6. This shows the results of maximum load (P_{max}) and the initial stiffness coefficient (K_i) for all the punch diameters. The initial stiffness was calculated from the first slope in the load-displacement curve presented in Figure 14.

Table 6. Numerical model results.

Fibres	Properties	D16	D30	D63
Basalt-FRCM	F_{max} (KN)	1.95	2.25	3.07
	Δ_{exp}	-13%	-5%	0%
	K_i (KN)	2.28	3.18	4.47

	Δ_{exp}	-40%	-14%	16%
Carbon-FRCM	F_{max} (KN)	2.38	2.78	3.97
	Δ_{exp}	-2%	1%	3%
	K_i (KN)	2.29	2.62	4.41
	Δ_{exp}	-41%	-26%	24%

Δ_{exp}: variation with the experimental results

The results presented in Table 6 show that maximum load results of the numerical model fit better the experimental results than the initial stiffness output.
Figure 14 show the contrast of the load-displacement diagrams of the experimental and numerical results. These demonstrate that the proposed numerical models are able to reproduce the experimental response with sufficient approximation. However, this numerical model is not capable to reproduce the sliding process. Including frictional and/or cohesive contacts may led to a more accurate model of the post-critic sliding response. Nevertheless, it is far beyond the scope of the current research.

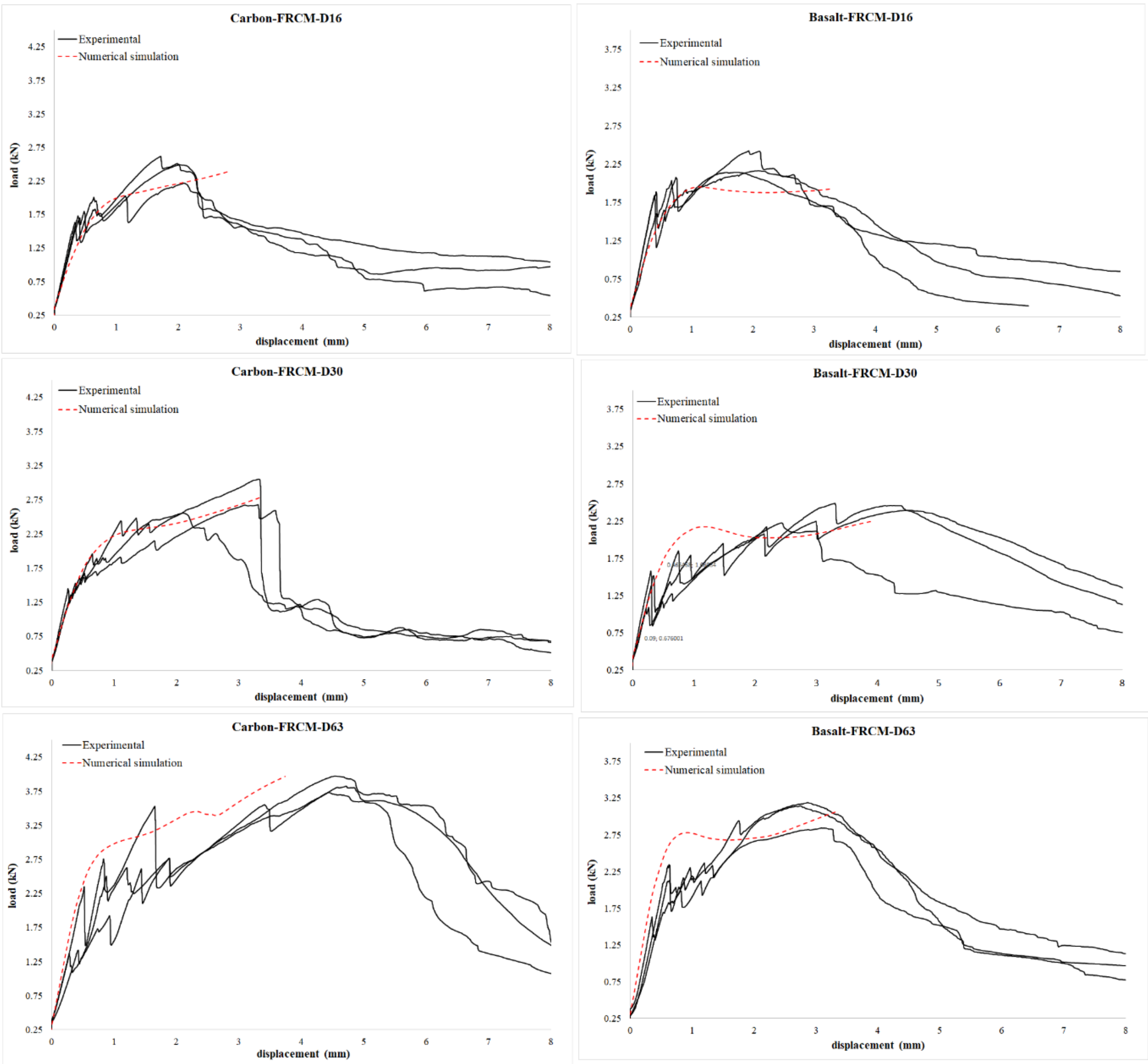

Figure 14. Contrast of the experimental and numerical load-displacement plots.

5 Conclusions

In this work, an experimental, analytical and numerical research was conducted to investigate the flexural performance of FRCM plates. According the achieved results:

- The basalt and carbon fabrics improve the flexural capacity in load and stiffness. Especially in the case of carbon-FRCM (D63) that improves 103% the maximum load.
- The carbon-FRCM presented fabric sliding failures and the basalt-FRCM presented fabric rupture failures. These types of failures were related to the degree of bonding behavior between the different materials (fabric-mortar).
- The maximum load increased with the increase of the punch diameter. However, the stiffness was not affected significantly by the increase of the punch diameter.
- The analytical and numerical analysis of FRCM may be performed similarly to reinforced concrete. Concrete formulations and models were useful to calculate the experimental results of this research.
- The mortar tensile strength and Young modulus were obtained from fitting the analytical calculation of the load-bearing capacity of mortar plates without fabrics. These values were successfully used to FRCM´s numerical simulation proving that unreinforced mortar properties are representative to the proposed model.
- The tensile sliding stress of the carbon fabric was obtained by comparing the experimentally determined maximum loads with the numerical results. The carbon fabric started to slide when it reached the 74 % of its tensile strength.
- The proposed numerical model was able to reproduce the experimental maximum load with sufficient approximation (between 0-13%). However, this numerical model is not yet capable to reproduce the sliding process.

Acknowledgements

Authors want to thanks the research project SEVERUS (RTI2018-099589-B-I00) of the Spanish Research Agency. Authors also want to acknowledge the support provided by Bernat Almenar Muns during experimental testing. Second author is a Serra Húnter Fellow.

References

[1] Torabian A, Isufi B, Mostofinejad D, Ramos AP. Behavior of thin lightly reinforced flat slabs under concentric loading. Eng Struct 2019;196. https://doi.org/10.1016/j.engstruct.2019.109327.

[2] Marí A, Cladera A, Oller E, Bairán JM. A punching shear mechanical model for reinforced concrete flat slabs with and without shear reinforcement. Eng Struct 2018;166:413–26. https://doi.org/10.1016/j.engstruct.2018.03.079.

[3] Lapi M, Ramos AP, Orlando M. Flat slab strengthening techniques against punching-shear. Eng Struct 2019;180:160–80. https://doi.org/10.1016/j.engstruct.2018.11.033.

[4] Ibrahim HM. Experimental investigation of ultimate capacity of wired mesh-reinforced cementitious slabs. Constr Build Mater 2011;25:251–9. https://doi.org/10.1016/j.conbuildmat.2010.06.032.

[5] Menétrey P. Synthesis of punching failure in reinforced concrete. Cem Concr Compos 2002;24:497–507. https://doi.org/10.1016/S0958-9465(01)00066-X.

[6] Babaeidarabad S, De Caso F, Nanni A. Out-of-Plane Behavior of URM Walls Strengthened with Fabric-Reinforced Cementitious Matrix Composite. Asce 2014;549:1–11. https://doi.org/10.1061/(ASCE)CC.

[7] Balsamo A, Di Ludovico M, Prota A, Manfredi G. Masonry walls strengthened with innovative composites. Am Concr Institute, ACI Spec Publ 2011;2:769–86.

[8] Raoof SM, Bournas DA. TRM versus FRP in flexural strengthening of RC beams: Behaviour at high temperatures. Constr Build Mater 2017;154:424–37. https://doi.org/10.1016/j.conbuildmat.2017.07.195.

[9] Younis A, Ebead U, Shrestha KC. Different FRCM systems for shear-strengthening of reinforced concrete beams. Constr Build Mater 2017;153:514–26. https://doi.org/10.1016/j.conbuildmat.2017.07.132.

[10] Minafò G, La Mendola L. Experimental investigation on the effect of mortar grade on the compressive behaviour of FRCM confined masonry columns. Compos Part B Eng 2018;146:1–12. https://doi.org/10.1016/j.compositesb.2018.03.033.

[11] Gattesco N, Boem I. Experimental and analytical study to evaluate the effectiveness of an in-plane reinforcement for masonry walls using GFRP meshes. Constr Build Mater 2015;88:94–104. https://doi.org/10.1016/j.conbuildmat.2015.04.014.

[12] Mercedes L, Bernat-Maso E, Gil L. In-plane cyclic loading of masonry walls strengthened by vegetal-fabric-reinforced cementitious matrix (FRCM) composites. Eng Struct 2020;221:111097. https://doi.org/10.1016/j.engstruct.2020.111097.

[13] D’Anna J, Amato G, Chen JF, Minafò G, La Mendola L. Effectiveness of BFRP confinement on the compressive behaviour of clay brick masonry cylinders. Compos Struct 2020;249:112558. https://doi.org/10.1016/j.compstruct.2020.112558.

[14] Di Ludovico M, Cascardi A, Balsamo A, Aiello MA. Uniaxial experimental tests on full-scale limestone masonry columns confined with glass and basalt frcm systems. J Compos Constr 2020;24:1–14. https://doi.org/10.1061/(ASCE)CC.1943-5614.0001061.

[15] Escrig C, Gil L, Bernat-Maso E, Puigvert F. Experimental and analytical study of reinforced concrete beams shear strengthened with different types of textile-reinforced mortar. Constr Build Mater 2015;83:248–60. https://doi.org/10.1016/j.conbuildmat.2015.03.013.

[16] Bernat-Maso E. Comportamiento estructural de muros de obra de fábrica reforzados con TRM. In: Perez MA, editor. Apl. Av. los Mater. compuestos en la obra Civ. y la Edif., 2013, p. 137–64. https://doi.org/10.1017/CBO9781107415324.004.

[17] Li W qian, Zhu JH, Chen P yu, Xing F, Li D, Su M. Evaluation of carbon fiber reinforced cementitious matrix as a recyclable strengthening material. J Clean Prod 2019;217:234–43. https://doi.org/10.1016/j.jclepro.2019.01.256.

[18] EN 1015-11:2019. Methods of test for mortar for masonry. Determination of flexural and compressive strength of hardened mortar. 2019.

[19] Mercedes L. Análisis del comportamiento frente acciones cíclicas de muros de mampostería reforzados con materiales compuestos de matriz inorgánica y

tejidos de fibras vegetales. Universidad Politécnica de Catalunya, 2019.

[20] Mercedes L, Gil L, Bernat-maso E. Mechanical performance of vegetal fabric reinforced cementitious matrix (FRCM) composites. Constr Build Mater 2018;175:161–73. https://doi.org/10.1016/j.conbuildmat.2018.04.171.

[21] Askouni PD, Papanicolaou C (Corina) G. Textile Reinforced Mortar-to-masonry bond: Experimental investigation of bond-critical parameters. Constr Build Mater 2019;207:535–47. https://doi.org/10.1016/j.conbuildmat.2019.02.102.

[22] Santandrea M, Focacci F, Mazzotti C, Ubertini F, Carloni C. Determination of the interfacial cohesive material law for SRG composites bonded to a masonry substrate. Eng Fail Anal 2020;111:104322. https://doi.org/10.1016/j.engfailanal.2019.104322.

[23] Aveston J, Kelly A. Theory of multiple fracture of fibrous composites. J Mater Sci 1973;8:352–62. https://doi.org/10.1007/BF00550155.

[24] BS EN 1992-1-1. Eurocode 2: Design of concrete structures - Part 1-1 : General rules and rules for buildings. Br Stand Inst 2004;1:230. https://doi.org/[Authority: The European Union Per Regulation 305/2011, Directive 98/34/EC, Directive 2004/18/EC].

[25] EHE-08. Normativa de hormigón estructural en España 2008;1:1689–99. https://doi.org/10.1017/CBO9781107415324.004.

[26] Simulia. Abaqus 6.11. User´s Manual 2011.

[27] Bertolesi E, Carozzi FG, Milani G, Poggi C. Numerical modeling of Fabric Reinforce Cementitious Matrix composites (FRCM) in tension. Constr Build Mater 2014;70:531–48. https://doi.org/10.1016/j.conbuildmat.2014.08.006.

[28] Alfarah B, López-Almansa F, Oller S. New methodology for calculating damage variables evolution in Plastic Damage Model for RC structures. Eng Struct 2017;132:70–86. https://doi.org/10.1016/j.engstruct.2016.11.022.

[29] Bertolesi E, Milani G, Poggi C. Simple holonomic homogenization model for the non-linear static analysis of in-plane loaded masonry walls strengthened with FRCM composites. Compos Struct 2016;158:291–307. https://doi.org/10.1016/j.compstruct.2016.09.027.

[30] Bernat-maso E, Gil L, Mercedes L, Escrig C. Mechanical properties of pre-stressed fabric-reinforced cementitious matrix composite (PFRCM). Constr Build Mater 2018;191:228–41. https://doi.org/10.1016/j.conbuildmat.2018.09.210.